Plasma Sources Science and Technology

PURPOSE-LED PUBLISHING™

LETTER • **OPEN ACCESS**

Controlling the breakdown delay time in pulsed gas discharge

To cite this article: I V Schweigert *et al* 2022 *Plasma Sources Sci. Technol.* **31** 03LT01

View the article online for updates and enhancements.

You may also like

- Streamer inception thresholds derived from a statistical electron transport model
Raphael Färber and Christian M. Franck
- Impact of overvoltage on the mode transition of the spark gap switch: from edge breakdown to stochastic breakdown
Weixi Luo, Chenhua Ren, Bangdou Huang et al.
- Gas breakdown in radio-frequency field within MHz range: a review of the state of the art
Wei JIANG, , Hao WU et al.

This content was downloaded from IP address 194.95.157.36 on 24/01/2025 at 07:52

OPEN ACCESS
IOP Publishing

Letters
Plasma Sources Science and Technology

Plasma Sources Sci. Technol. **31** (2022) 03LT01 (9pp)
https://doi.org/10.1088/1361-6595/ac417a

Letter

Controlling the breakdown delay time in pulsed gas discharge

I V Schweigert[1,2,*], M M Hopkins[3], E Barnat[3] and M Keidar[1]

[1] George Washington University, Washington, DC 20052, United States of America
[2] Khristianovich Institute of Theoretical and Applied Mechanics, Novosibirsk 630090, Russia
[3] Sandia National Laboratories, Albuquerque, NM, United States of America

E-mail: ivschweigert@gmail.edu

Received 10 August 2021, revised 29 November 2021
Accepted for publication 9 December 2021
Published 29 March 2022

Abstract

In experiment and 2D3V PIC MCC simulations, the breakdown development in a pulsed discharge in helium is studied for $U = 3.2$ kV and 10 kV and $P = 100$ Torr. The breakdown process is found to have a stochastic nature, and the electron avalanche develops in different experimental and simulation runs with time delays ranging from 0.3 to 8 μs. Nevertheless our experiments demonstrate that the breakdown delay time distribution can be controlled with a change of the pulse discharge frequency. The simulation results show that the breakdown process can be distinguished in three stages with (a) the ionization by seed electrons, (b) the ions drift to the cathode and (c) the enhanced ionization within the cathode sheath by the electrons emitted from the cathode. The effects of variation of seed electron concentrations, voltage rise times, voltage amplitudes and ion–electron emission coefficients on the breakdown development in the pulsed gas discharge are reported.

Keywords: Gas discharge, breakdown delay time, electron emission

(Some figures may appear in colour only in the online journal)

Gas discharge breakdown is the process of converting a neutral gas into a highly conductive state under the voltage, which typically takes from 10^{-9} s to 10^{-4} s. An electron avalanche can be initiated by electrons remaining from previous voltage pulses, emitted from electrodes or supplied by the external plasma sources [1, 2]. The breakdown scenario in a gas discharge is a fundamental problem considered in experimental and theoretical studies (see, for example, [3, 4]), but some questions remain open. Requirements for the breakdown parameters of plasma sources such as the times of the exponential discharge current rise, τ_s, and breakdown delay, τ_d, shown in figure 1 are various for different applications. The record subnanosecond current rise time τ_s was achieved in a high-voltage pulsed discharge with counter-propagating electron beams at $P = 5$–30 Torr [5, 6]. This type of breakdown develops within 0.1–0.5 ns and governed by photoemission from the cathodes with the resonant photons with a Doppler shifted frequency. The breakdown delay time τ_d in these gas-discharge devices was controlled with a capillary discharge built into the main discharge chamber [7]. The τ_d ranged from 0.2 to 2 μs for a discharge frequency up to 100 kHz and a discharge current up to 1 kA.

In this study, our experiments on the ignition of pulsed gas discharge at gas pressures of 100 Torr and $U = 3.2$ kV showed a wide distribution of breakdown delay time. The multiple attempts to ignite the discharge for the same initial conditions

* Author to whom any correspondence should be addressed.

Original content from this work may be used under the terms of the Creative Commons Attribution 4.0 licence. Any further distribution of this work must maintain attribution to the author(s) and the title of the work, journal citation and DOI.

 © 2022 The Author(s). Published by IOP Publishing Ltd Printed in the UK

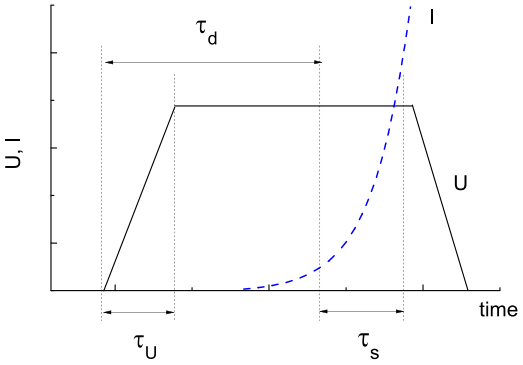

Figure 1. Characteristic times of exponential discharge current rise, τ_s, breakdown delay, τ_d, and voltage front increase, t_U.

gave a set of breakdown delays ranging from 1 to 10 μs. Nevertheless, our observations showed that the breakdown delay time is sensitive to a variation of the time of the voltage front increase, t_U, and an increase of the frequency of voltage pulses. In this letter, we will focus on the experimental and kinetic study of the breakdown scenario in a pulsed gas discharge in helium at $P = 100$ Torr and a voltage amplitude of 3.2 kV and 10 kV.

Experimental setup. In our experiment, the discharge environment is generated in a vacuum chamber that is evacuated to medium pressures of 0.01 Torr. After evacuation, the chamber is subsequently backfilled with UHP grade helium using a continual helium flow rates that is set to 200 SCCM resulting in target pressure of 100 Torr. As monitored by the equilibrium chamber pressure prior to the introduction of helium, it is noted that the injected flow rates far exceed the chamber leak rate and the outgassing rates of materials in the chamber by a factor of 100 or more. Therefore, it is anticipated that the impurity level is less 0.01% of the total gas environment.

The electrical breakdown occurs in the helium environment between two planar electrodes shown in figure 2(a). The 10 cm diameter cathode consists of an aluminum chuck with a highly doped conductive silicon wafer coated with 100 nm thick (electron beam-deposited) platinum film. We used that to ensure there was a good electrical contact between the electrode and the Pt film. The anode is an annular disc that contains a 2.5 cm diameter flat central disc and is curved or flared around the 3 cm outer diameter. The flare is introduced to reduce electric filed strength at the edge of the discharge that would be present had the anode possessed sharp corners. For our study, the anode to cathode gap distance is 1.2 cm.

The breakdown is initiated by placing a voltage between the anode and the cathode. The anode is connected to the high voltage supply while the cathode is connected to ground via a 10 Ohm current sensing resistor. For discharge initiation, a voltage pulse is applied to the anode using a DEI high voltage pulser. The switching of the voltage is driven by a TTL pulse of varying frequency and fixed width of 10 μs provided by a SRS645 digital delay generator. Voltage and current signatures are captured with a high resolution (12 bit) high speed (1 GHz) digitizing oscilloscope (LeCroy HDO4100). The oscilloscope

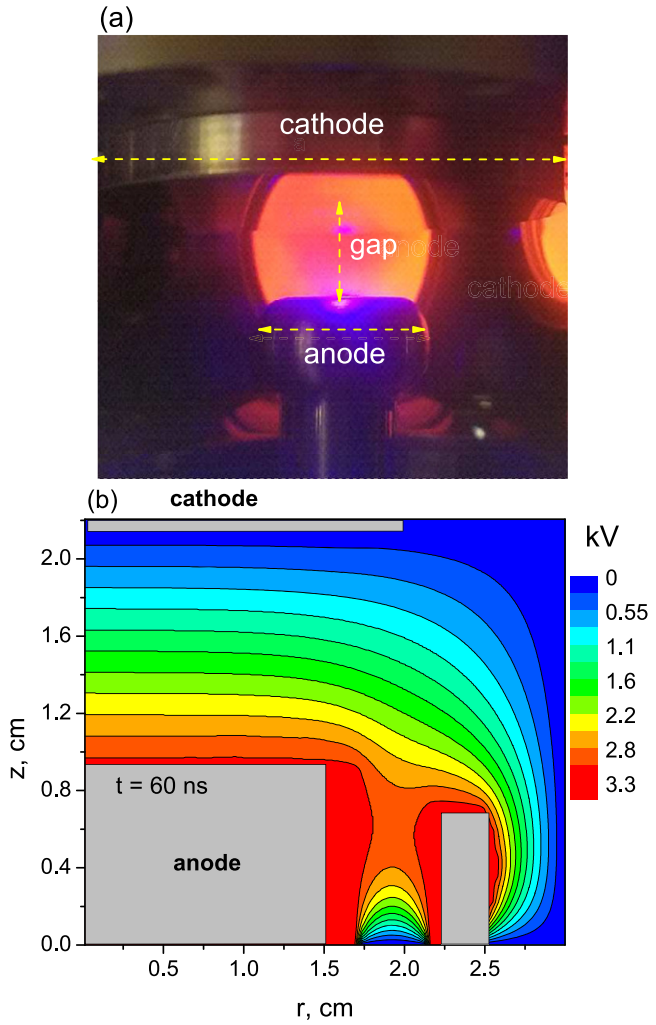

Figure 2. Photo of gas discharge operating in helium between electrodes (a) and simulation domain with calculated electric potential distribution in the first stage of the breakdown at $t = 40$ ns (b).

is triggered by the digital delay generator that initiates the breakdown process. The 10 Ohm resistor in combination with a 2 mV/division scale (200 mV full scale) produces a baseline sensitivity of 5 μA. Prior to making the measurements reported in this study, the discharge system is conditioned by performing over 20 000 breakdown events at a rate of 20 Hz for 20 min. During the conditioning process, it is observed that breakdown delays are increased with increasing operation. We determine that the system is conditioned when there is no longer any observed change in the breakdown delay time distribution.

Simulation details. The kinetic simulations of dynamics of discharge plasma are performed with the 2D3V particle-in-cell Monte Carlo collision method (PIC MCC). The kinetic equations for the electron and ion distribution functions are solved self-consistently with the Poisson equation for the electric potential distribution. The collision set for electrons [8, 9] includes the elastic scattering, excitation and ionization of He background atoms. For the ions, the resonant charge exchange

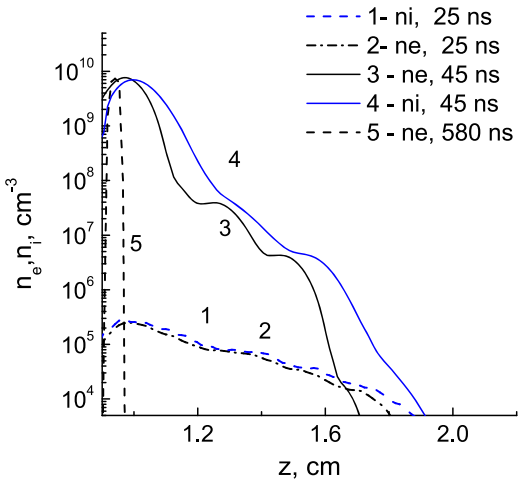

Figure 3. Electron and ion density distributions at $r = 0$ in the first stage of discharge breakdown, $n_0 = 10^3$ cm^{-3}, $t_U = 40$ ns.

collisions with background atoms, or backward elastic scattering are taken into account.

The initial distributions of electron and ions densities at $t = 0$ when the voltage starts to increase are calculated with solving the kinetic equations and Poisson equation at $U = 0$. First we took an uniform initial profile of quasineutral plasma and let the system to relax to different maximum of n_0.

For accurate calculations of electron dynamics we choose the electron time step $\Delta t_e \ll 1/\omega_p, 1/\omega_s, \Delta r/v_e, \Delta z/v_e$, where ω_p is the plasma frequency, ω_s is the electron scattering frequency with the background atoms, Δr, Δz are steps of calculation grid over axes r and z, and v_e is the maximum electron velocity [6, 15–17]. Prior to the breakdown study in simulations, we performed test runs, checking the effects of time and grid step variation on the accuracy of the results. For our experimental conditions, the plasma frequency ω_p is about 2×10^{10} s^{-1}, the frequency of electron scatterings with the background atoms $\omega_s = 2 \times 10^{11}$ and $\Delta z/v_e < 5 \times 10^{-12}$ s. In simulations, the electron time step Δt_e is $(0.5–5) \times 10^{-14}$ s. The calculation grid is nonuniform over z-direction condensing within the cathode sheath. Over axis r the calculation grid is uniform over $r < 1.5$ cm and become a more disperse with r. The total number of pseudo particles being chosen so that there is an average of approximately 100 positive and negative particles per Debye sphere. In simulations, the number of pseudo particles is renormalized to limit the exponential growth of the number of particles during the breakdown.

The experimental and model discharge chambers are shown in figure 2. In simulations, the cylindrical chamber has the height $H = 2.2$ cm and the radius $R = 3.5$ cm, and is solved in axisymmetric coordinates. The cathode radius is 2 cm (5 cm in the experiment) and the anode radius is 1.5 cm (1.5 cm in the experiment) and the distance from the cathode to the anode is 1.2 cm (1.2 cm in the experiment). In simulations, a guide ring is placed around the anode to avoid an enhancement of the electric field on the sharp edge.

The voltage applied to the anode increases linearly from zero to a maximum value of 3.2 kV or 10 kV during $t_U = 20$, 40 or 200 ns in different calculation runs. The electron emission from the cathode due to the ion bombardment is included in consideration, and the ion–electron emission coefficient $\gamma = 0.01–0.05$. The probability of ion–electron emission from the cathode surface is calculated with a random number, when an ion collides the surface. For our experimental conditions the plasma is optically dense for resonant photons (He $2^1P \rightarrow 2^1S$ resonance radiation). The cross section of reabsorption of resonant photons with a wavelength of $\lambda = 58.4334$ nm is about 10^{-13} cm^2, and the lifetime in the excited state is 0.56 ns [10]. The estimated time for the photons to reach the surface is much longer than 10 μs. The line broadening due to the finite lifetime of the excited states, interaction of the radiating atom with the surrounding atoms, Stark-effect, Doppler mechanism [11, 12] is negligible for our discharge parameters. For a different range of discharge parameters the photoemission contribution in the electron avalanche can be more important. In PIC MICC simulations, Donkó *et al* [13] studied the plasma and resonant photon transport in helium microdischarges with nanosecond kV voltage pulse using the approach of Fierro *et al* [14]. The results of PIC MICC simulations reported in reference [13] showed that the discharge current increased by a factor of two with accounting for the photoemission. Nevertheless the strong trapping of resonant photons was observed, and the photon flux to the cathode was delayed and smaller compared to the ion flux. The discharge current increased during 10–15 ns with and without accounting for UV photons. The dominant role of photoemission was reported in references [5, 6] in the pulsed open discharge with the voltage of 20 kV and the gas pressure of 6 Torr. The high densities of fast atoms and fast ions provided an essential Doppler shift in the frequencies of the resonant photons allowing them to propagate with a speed of light as in the vacuum. These Doppler shifted photons provided a subnanosecond breakdown time [6].

In the experiments, the pulse discharges ignition is registered for the operation frequency of 1–40 Hz. In figure 1, the schematic voltage–current behavior is shown. In the experiment, the voltage pulse duration is more than 100 μs. In simulations, the voltage increases from zero to the maximum value U_0 during time τ_U and then $U = U_0$. Various initial plasma densities, n_0, were taken to mimic the afterglow plasma between voltage pulses at different frequencies, and n_0 ranges from 10^2 to 10^4 cm^{-3}. In most calculations, the voltage rise time t_U is 40 ns and $U = 3.2$ kV, unless otherwise specified.

First stage of the breakdown. Initially, with increasing voltage, the potential distribution is almost linear (see figure 2(b)) since n_0 is low over the interelectrode gap. The seed electrons are accelerated to the anode direction gaining the energy in the electric field and ionizing the background helium gas. In figure 3, the profiles of electron and ion densities, n_e, n_i, at the axis of symmetry are shown for different times for $n_0 = 10^3$ cm^{-3} and $t_U = 40$ ns. During the first 25 ns of voltage rise, the plasma density n increases by two orders of magnitude, and at $t = 45$ ns the n reaches a maximum of 10^{10} cm^{-3}. After 100–300 ns almost all electrons escape from the discharge volume to the anode and the ionization stops. Note that the plasma is practically quasineutral at $t = 45$ ns, but

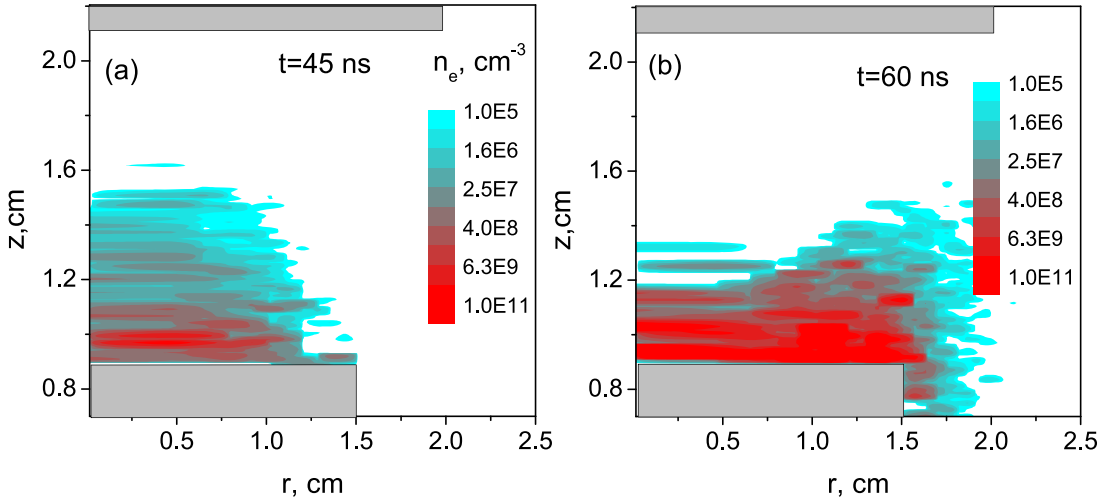

Figure 4. Spatial distribution of electron density for $t = 45$ ns (a) and 60 ns (b), $n_0 = 10^3$ cm^{-3}.

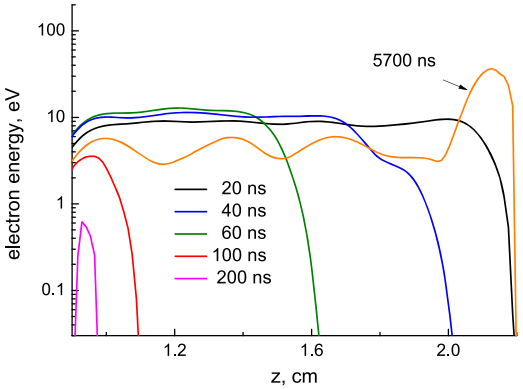

Figure 5. Electron energy profiles at $r = 0$ for different times.

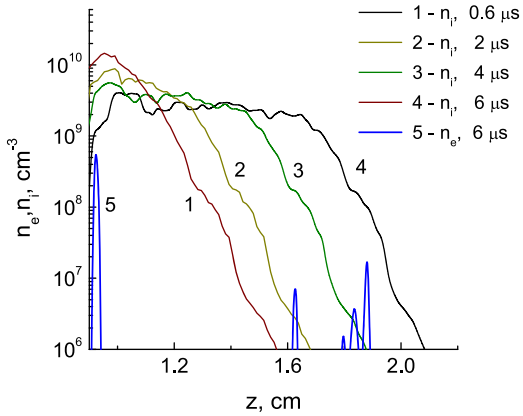

Figure 6. Ion and electron density distribution at $r = 0$ in the second stage for $n_0 = 10^3$ cm^{-3}.

at $t \geqslant 300$ ns only the positive ions remain in the discharge gap, with the exception of a thin layer of cold electrons captured by the potential dip near the anode surface (see figure 3).

The spatial distributions of the electron density for this case shown in figure 4 at $t = 45$ ns and 60 ns illustrate the electron dynamics. The volume ionization ν_i varies within a range of (1–5) $\times$ 10^{16} cm^{-3} s^{-1} and is provided by the electrons with the mean energy ϵ_e of 10–12 eV.

In figure 5, the electron energy profiles are shown for different times. The electron energy quickly decreases for $t > 80$ ns and drops to 0.6 eV for $t = 200$ ns.

The first stage of the breakdown development ends with a drop of the electron energy. This stage is associated with the ionization process by seed electrons and lasts for 100–300 ns.

Second stage of the breakdown. At this stage, the ions drift toward the cathode with an almost constant average velocity (1–2) $\times$ 10^5 cm s^{-1}, as shown in figure 6. At $t =$ 6 μs the flux of ions to the cathode surface is still small, but the spikes of the electron density in figure 6 indicate that a few electrons were emitted by ions hitting the cathode. The absence of electron avalanche can be explained with a comparison of the electron ionization mean free path λ_i and the inter-electrode gap length. The cross section for ionization of He atoms by electron impact is very small for an electron mean energy of 10 eV, $\sigma_i < 10^{-19}$ cm^2. This means that $\lambda_i > 3$ cm, whereas the inter-electrode gap is 1 cm. For an electron, the mean free path between collisions is a stochastic value, and a significant number of emitted electrons is needed for the coupling of the emitted electrons and the ion flux within a narrowing cathode sheath. This coupling provides an exponential rise of the discharge current.

Third stage of the breakdown. This final stage of the breakdown is related to an enhancement of the current of electrons emitted from the cathode. The ions delivered during the second stage sweep the cathode surface, the cathode sheath becomes narrower and the electric field increases. In figure 7, the distributions of the electric field E_z and the discharge current density are shown at $t = 7$ μs for the case of the breakdown delay time $\tau_d = 7.3$ μs. The mean energy of electrons after the crossing the cathode sheath is 100 eV at $t = 7$ μs. With an increase of electron energy, the ionization mean free path λ_i diminishes and the ionization rate within the cathode sheath quickly increases. For an example, for the electron with $\epsilon_e = 50$ eV, $\lambda_i = 0.0126$ cm and for $\epsilon_e = 100$ eV,

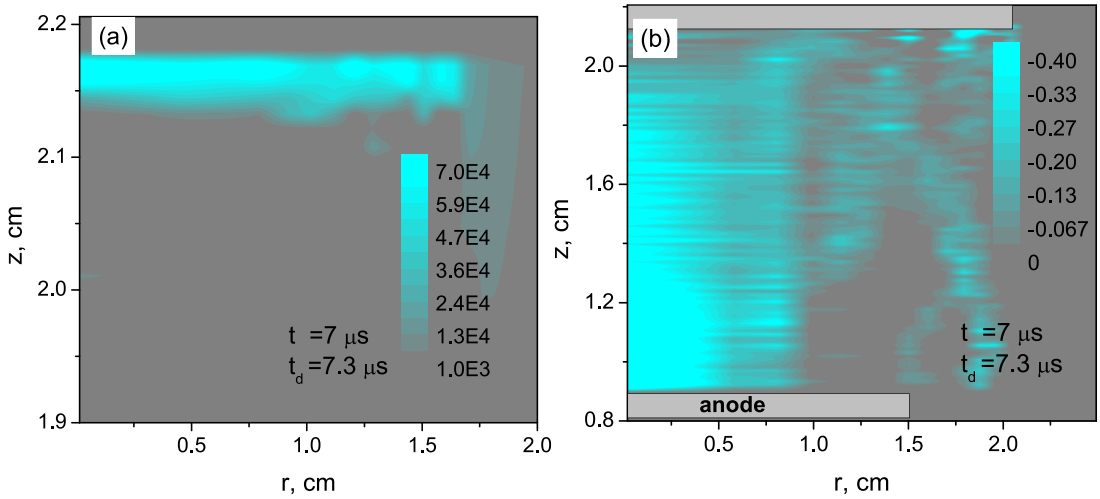

Figure 7. Spatial distributions of (a) electric field, E_z (V cm^{-1}) and (b) discharge current density (A cm^{-2}) at $t = 7$ μs for the case of the breakdown delay time $\tau_d = 7.3$ μs, $t_U = 40$ ns, $n_0 = 10^2$ cm^{-3}.

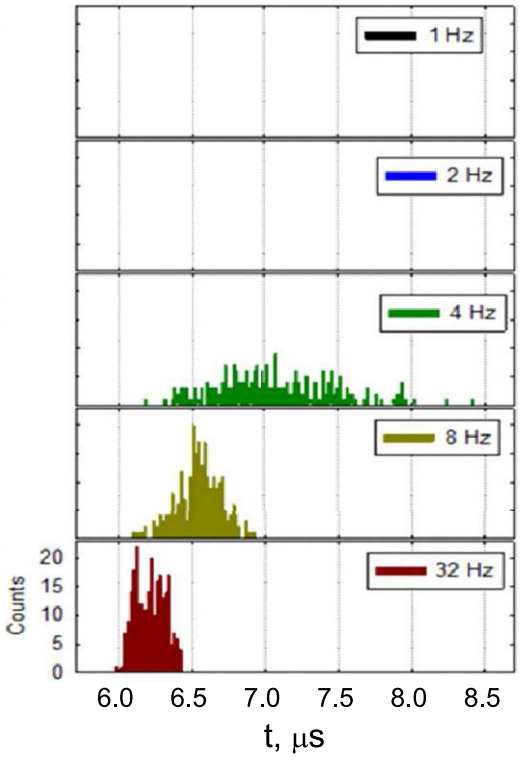

Figure 8. Measured breakdown delay time for different voltage frequencies. The data were obtained over 100 shots at each frequency.

$\lambda_i = 0.0086$ cm. The ionization within the cathode sheath enlarges the ion flux to the cathode and enhances the current of emitted electrons, which starts to grow exponentially.

PIC MCC method allows us to track all groups of electrons with different energies without special modification of algorithm. At our gas pressure of 100 Torr, the electron mean free path λ_i is less than 0.1 cm for $\epsilon_e = 100$–$10\,000$ eV, since $\sigma_i \geqslant 3 \times 10^{-18}$ cm^2 for $\epsilon_e \leqslant 10$ keV. Therefore we did not see runaway electrons in our simulations even in the third stage of the breakdown.

Breakdown delay. In the experiment, the time of the breakdown delay, τ_d, measured in different runs exhibits a wide distribution. An increase of the voltage pulse frequency leads to a narrowing of the distribution of τ_d. Figure 8 shows the experimental data on the breakdown delay time distribution for the voltage frequencies f ranged from 1 Hz to 32 Hz. For $f = 1$ and 2 Hz, no discharge breakdown was observed on the time scales considered here. In the experiment, we registered the following breakdown delay times: for $f = 4$ Hz, 6.2 μs $< \tau_d <$ 8 μs, for $f = 8$ Hz, 6.1 μs $< \tau_d <$ 7 μs and for $f = 32$ Hz, 6 μs $< \tau_d <$ 6.4 μs. Thus a spread of τ_d decreases from 1.8 μs to 0.4 μs with f decrease from 4 Hz to 32 Hz. In figure 9, the calculated discharge current with time is shown for the initial plasma densities $n_0 = 10^2$ cm^{-3} and 10^4 cm^{-3}. Note, that j_d is shown with the same time scale of 2.2 μs for both cases. The results of modeling the evolution of the discharge current for various initial plasma densities demonstrate the same tendency as in the experiment, the lower the initial density, the wider distribution of the breakdown time delay. The spread of τ_d decreases from 0.9 μs to 0.5 μs when n_0 increases from 10^2 cm^{-3} and 10^4 cm^{-3}. The delay time of the breakdown, τ_d, is defined as a time when the discharge current $j_d = 0.06$ A, that is less than 30% of the maximum value of j_d.

Effect of the voltage rise time for different voltages. In simulations, we found that a decrease of the voltage rise time, t_U, and an increase of the discharge frequency similarly affect the τ_d distribution. Both provide a higher plasma density in the first stage of the breakdown, which narrows the τ_d distribution. Let us consider the influence of t_U on the plasma density profile in the end of the first stage for $t = 230$ ns, when the ionization by seed electrons stops. Four cases with the voltage rise time, $t_U = 200$ ns and 20 ns and $U = 3.2$ kV and 10 kV were analyzed. The n_e, n_i distributions and the potential profiles for these cases are shown in figure 10 for $t \approx 230$ ns. It is seen in figure 10(a), that for $U = 3.2$ kV and

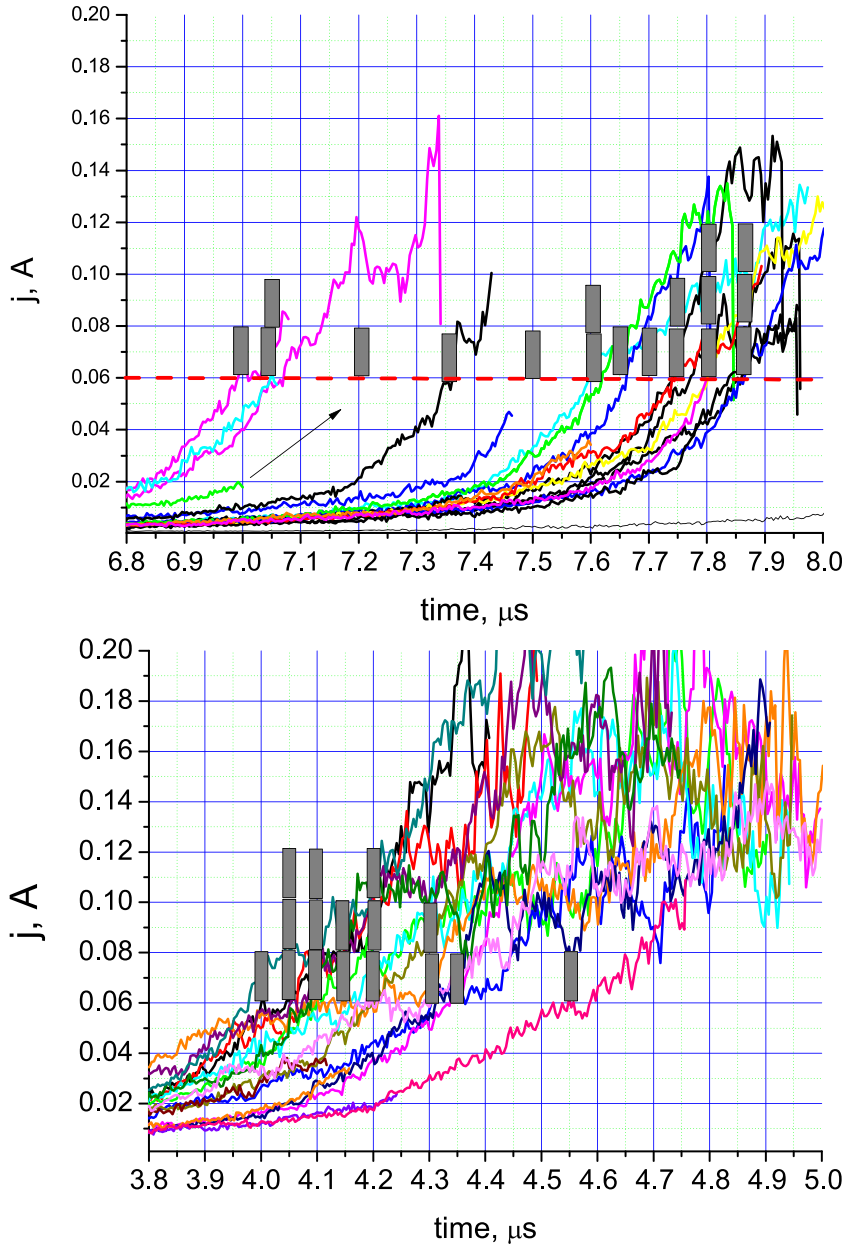

Figure 9. Calculated discharge current evolution, $t_U = 40$ ns, for $n_0 = 10^2$ cm^{-3} (top) and 10^4 cm^{-3} (bottom).

$t_U = 200$ ns, the plasma density is low, $n < 4 \times 10^7$ cm^{-3} since the seed electrons escape from the discharge volume during the first 80 ns. For the case of $t_U = 20$ ns, the n is considerable larger, $n < 1.6 \times 10^{10}$ cm^{-3}. For $t_U = 200$ ns the electric potential has a linear distribution and for $t_U = 20$ ns a thin quasineutral plasma layer forms near the anode (see figure 10(b)). For a higher voltage of $U = 10$ kV and $t_U = 200$ ns, the plasma distribution is similar to the case of $U = 3.2$ kV, $t_U = 20$ ns, but E/N is larger and a more narrow τ_d distribution can be expected. For 10 kV and $t_U = 20$ ns, the plasma density is $n \approx 4 \times 10^{11}$ cm^{-3}, and an extended plateau in the potential profile shows a zone of quasineutral plasma near the anode (figures 10(b) and (c)). For this case, the cathode sheath l is of 0.4 cm and this l is smaller in comparison with the cathode sheathes in the other three cases. Therefore the electric field, the ion concentration and mean velocity are larger and $\tau_d < 300$–400 ns.

The effect of t_U on the n in the first stage of the breakdown can be explained with a comparison of the ionization frequency ν_i and the frequency of the electron escape from the discharge volume, $\nu_{es} = v_e/d$, where v_e is the mean electron velocity in given E/P and d is the anode to cathode gap. For $U = (3.2$–$10)$ kV, $\nu_i/\nu_{es} = \sigma_i N d \approx 1$–$50$, where σ_i is the ionization cross section and N is the gas density. The characteristic time of the electron departure from the discharge volume is ≈20 ns for $U = 3.2$ kV and 6 ns for 10 kV. Therefore with increasing t_U to 200 ns a large portion of electrons escape from the discharge gap before the E/N reaches the threshold for the

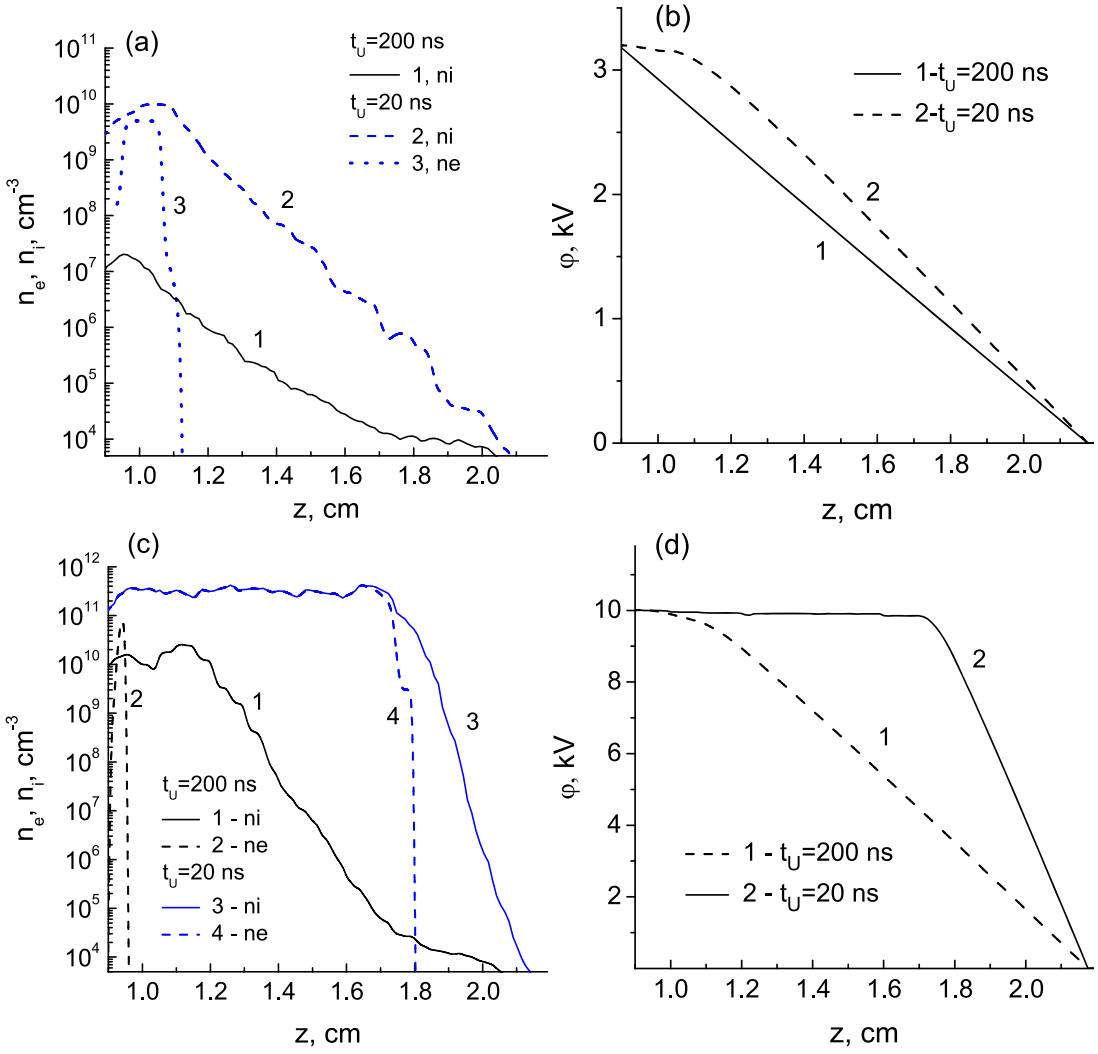

Figure 10. Profiles of electron and ion densities (a), (c) and electric potential (b), (d) for $t_U = 20$ ns and 200 ns at $t = 230$ ns for $U = 3.2$ kV (a), (b) and $U = 10$ kV (c), (d), $n_0 = 10^4$ cm^{-3}.

ionization. Thus, the ionization is limited by the escape of seed electrons during the rise of the voltage front. It is seen in figures 10(c) and (d), that for $U = 10$ kV and $t_U = 20$ ns, the quasineutral plasma forms faster than the electrons depart from the discharge, since $\nu_i \gg \nu_{es}$.

Effect of ion–electron emission. A value of electron yield from the cathode surface is one of the key parameters which determines the breakdown process. The coefficient of ion–electron emission γ can be influenced by choosing the material of the cathode, processing or environment. For a small γ the electron avalanche does not develop for our experimental conditions. The ion current to the cathode with time is shown in figure 11 for $\gamma = 0.05$ and $\gamma = 0.01$. In the former case, the breakdown happens at $t = 6$ μs, and in the latter case, no breakdown was observed.

In this study, we used the simplified model of the electron emission from the cathode surface. Only ion–electron emission was taken into account. For our experimental conditions, the breakdown delay time is determined by the first and second stages of breakdown development. At the first stage of the breakdown, the ionization and excitation rates by seed electrons are comparably low and during the second stage there is no ionization. In the third stage of the breakdown, when the

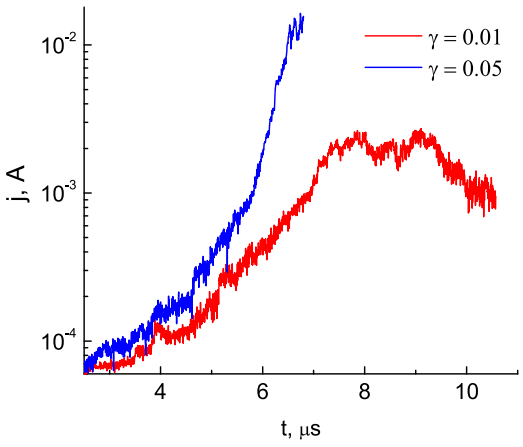

Figure 11. Discharge current for $\gamma = 0.01$ and 0.05 for $n_0 = 10^3$ cm^{-3}.

ionization quickly increases near the cathode surface the flux of resonant photons can contribute to the exponential growth of the emission current, but it does not affect the breakdown delay time. The resonant photons generated during the third stage of the breakdown do not participate in the electron avalanche of the next voltage pulse since the time gap between voltage pulses in our experiment is 0.1 s and all photons escape from the plasma volume.

In conclusion, the breakdown development in the pulsed discharge in helium with $U = 3.2$ kV and $P = 100$ Torr has been studied in the experiment and in 2D3V PIC MCC simulations. In the experiment, the time delay of the breakdown has been measured for 100 experimental trials at each shot frequency ranged from 1 Hz to 32 Hz. These measurements exhibited a wide distribution of the time delay of discharge ignition τ_d. An increase of pulse discharge frequency from 1 Hz to 32 Hz reduced a spread of τ_d. In 2D3V PIC MCC simulations, the dynamics of the discharge was studied for the experimental conditions and the geometry of the plasma chamber with the different (a) initial plasma densities, (b) voltage rise times, (c) voltage amplitudes and (d) ion–electron emission coefficients.

The simulation results showed that the discharge breakdown process undergoes three different stages. In the first stage, with increasing voltage from $U = 0$ to the maximum amplitude, the seed electrons from a previous pulse are accelerated in the electric field to the anode direction. The ionization by the seed electrons essentially enlarges the plasma density. The first stage finishes when the electrons either escape from the discharge volume or thermalize and are trapped in the plasma quasineutral zone. During the second stage, the ions drift to the cathode direction, and the ionization is absent. This stage lasts about 5–8 μs for $U = 3.2$ kV both in the experiment and simulations. The third stage is related to a quick rise of the current of emitted electron current due to an increase of ion flux to the cathode. The ionization by emitted electrons takes place within the cathode sheath which becomes narrower with the coupling of the fluxes of ions and emitted electrons. In experiments and in simulations, the discharge current increases to 0.1–0.4 A. The breakdown delay time has a wide distribution over time since it is set by a probability processes such as an electron emission due to the ion bombardment and an electron stochastic ionization free path.

The breakdown process have been shown to have a stochastic nature with the time delay τ_d of 0.3–10 μs for $U = 3.2$ and 10 kV. A spread of τ_d was found to decrease with enlarging the applied voltage or the voltage frequency, lowering the time of voltage front rise, or choosing the cathode material with a higher electron yield. Our general findings from experimental and simulation results presented in the letter are (a) the occurrence of a wide distribution of the breakdown delay time because of a stochastic nature of electron kinetic processes and (b) possible ways to control the breakdown delay time. We have described the scenario of discharge breakdown process and the calculated distribution of breakdown delay time agreed with the experimental one. In PIC MCC simulations, it was shown that a steeper front of voltage rise, an increase of the voltage amplitude or frequency give the same effect of narrowing the τ_d spread. Thus, in pulsed gas discharges with parameters close to ours discussed above, one should expect a breakdown delay which can vary within microseconds. However, this breakdown delay time distribution can be controlled.

Acknowledgments

We wish to thank National Science Foundation Industry/University Cooperative Research Center for financial support. One of the authors, IS, was supported financially from Russian Science Foundation, Grant No. 22-49-08003 for the development of the simulation algorithm. This work was supported by the National Science Foundation under Grant No. 1747760. Sandia National Laboratories is a multimission laboratory managed and operated by National Technology and Engineering Solutions of Sandia, LLC, a wholly owned subsidiary of Honeywell International Inc., for the US Department of Energy National Nuclear Security Administration under Contract DE-NA0003525. We also wish to thank Amanda Lietz for participation in discussions. This paper describes objective technical results and analysis. Any subjective views or opinions that might be expressed in the paper do not necessarily represent the views of the US Department of Energy or the United States Government.

Data availability statement

All data that support the findings of this study are included within the article (and any supplementary files).

ORCID iDs

I V Schweigert https://orcid.org/0000-0002-2364-1228
M M Hopkins https://orcid.org/0000-0002-9620-7190
M Keidar https://orcid.org/0000-0003-0869-4310

References

[1] Raizer Y P 1991 *Gas Discharge Physics* (Berlin: Springer)
[2] Liberman M A, Groot J S D, Toor A and Spielman R B 1999 *Physics of High-Density Z-Pinch Plasmas* (Berlin: Springer)
[3] Hartmann P, Donkó Z, Bánó G, Szalai L and Rózsa K 2000 *Plasma Sources Sci. Technol.* **9** 183
[4] Jelenkovic B M and Phelps A V 2005 *Phys. Rev.* E **71** 016410
[5] Bokhan P A, Gugin P P, Zakrevsky D E and Lavrukhin M A 2013 *Tech. Phys. Lett.* **39** 775
[6] Schweigert I V, Alexandrov A L, Zakrevsky D E and Bokhan P A 2014 *Phys. Rev.* E **90** 051101(R)
[7] Bokhan P A, Belskaya E V, Gugin P P, Lavrukhin M A, Zakrevsky D E and Schweigert I V 2020 *Plasma Sources Sci. Technol.* **29** 084001

[8] Alves L L *et al* 2013 *J. Phys. D: Appl. Phys.* **46** 334002
[9] Yu R, Janev R K, Kato T, Fursa D V, Bray I and de Heer F J 2008 *At. Data Nucl. Data Tables* **94** 603
[10] Žitnik M, Stanič A, Bučar K, Lambourne J G, Penent F, Hall R I and Lablanquie P 2003 *J. Phys. B: At. Mol. Opt. Phys.* **20** 4175
[11] Holstein T 1951 *Phys. Rev.* **83** 1159
[12] Kunze H-J 2009 *Introduction to Plasma Spectroscopy* (Berlin: Springer)
[13] Donkó Z, Hamaguchi S and Gans T 2018 *Plasma Sources Sci. Technol.* **27** 054001
[14] Fierro A, Moore C, Scheiner B, Yee B T and Hopkins M M 2017 *J. Phys. D: Appl. Phys.* **50** 065202
[15] Birdsall C K and Langdon A B 1985 *Plasma Physics via Computer Simulation* (New York: McGraw-Hill)
[16] Birdsall C K 1991 *IEEE Trans. Plasma Sci.* **19** 65
[17] Schweigert I V, Alexandrov A L, Bokhan P A and Zakrevsky D E 2015 *Plasma Sources Sci. Technol.* **24** 044005